



This is a repository copy of *An analytic model for tube bending springback considering different parameter variations of Ti-alloy tubes*.

White Rose Research Online URL for this paper:
<http://eprints.whiterose.ac.uk/103638/>

Version: Accepted Version

Article:

Zhan, M., Wang, Y., Yang, H. et al. (1 more author) (2016) An analytic model for tube bending springback considering different parameter variations of Ti-alloy tubes. *Journal of Materials Processing Technology*, 236. pp. 123-137. ISSN 0924-0136

<https://doi.org/10.1016/j.jmatprotec.2016.05.008>

Reuse

This article is distributed under the terms of the Creative Commons Attribution-NonCommercial-NoDerivs (CC BY-NC-ND) licence. This licence only allows you to download this work and share it with others as long as you credit the authors, but you can't change the article in any way or use it commercially. More information and the full terms of the licence here: <https://creativecommons.org/licenses/>

Takedown

If you consider content in White Rose Research Online to be in breach of UK law, please notify us by emailing eprints@whiterose.ac.uk including the URL of the record and the reason for the withdrawal request.



eprints@whiterose.ac.uk
<https://eprints.whiterose.ac.uk/>

ELSEVIER

An analytic model for tube bending springback considering different parameter variations of Ti-alloy tubes

^aMei Zhan, ^a Yan Wang, ^{a*} He Yang, ^b Hui Long

^a State Key Laboratory of Solidification Processing, School of Materials Science and Engineering, Northwestern Polytechnical University, Xi'an 710072, PR China

^b Department of Mechanical Engineering, The University of Sheffield, Sheffield S1 3JD, UK

*Corresponding author. E-mail address: yanghe@nwpu.edu.cn (H. Yang).

Abstract

Springback after unloading is an issue that directly reduces the accuracy of bent tubes, especially for Ti-alloy tubes which are of high strength and low Young's modulus. The Young's modulus, E ; wall thickness, t ; and neutral layer, D_e , of a tube vary during the bending process. These variations may influence the bending deformation of components, thus on springback. Considering these variations, an analytic elastic-plastic tube bending springback model was established in this study based on the static equilibrium condition. When these variations were considered individually or combined, the resulting springback angles were all larger and closer to the experimental results than the results when variations were not considered for a $D_6 \text{ mm} \times t_0.6 \text{ mm}$ Ti-3Al-2.5V Ti-alloy tube. The t variation contribution is the large stand decreases the prediction error by 41.2%–45.3%. D_e variation ranks second and decreases the error by 21.2%-25.3%. E variation is the least significant, decreasing the error by only 2.4%. Furthermore, the influence of the stable Young's modulus E_a on the springback is larger than the initial Young's modulus E_0 . Therefore, for the bending springback of tubes with a small difference between E_0 and E_a and under a normal bending radius, E variation effects can be neglected. While for tubes with large differences between E_0 and E_a , and high springback prediction requirements, the E variation should be replaced by E_a . The influences of the initial tube sizes, material properties and bent tube sizes of the Ti-3Al-2.5V tube on springback were obtained using the newly developed model.

An analytic model for tube bending springback considering different parameter variations of Ti-alloy tubes

Mei Zhan^a, Yan Wang^a, He Yang^{a,*}, Hui Long^b

^a State Key Laboratory of Solidification Processing, School of Materials Science and Engineering, Northwestern Polytechnical University, Xi'an 710072, PR China

^b Department of Mechanical Engineering, The University of Sheffield, Sheffield S1 3JD, UK

* Corresponding author: Tel: +86-029-88495632; Fax: +86-029-88495632;

E-mail: yanghe@nwpu.edu.cn (H. Yang)

Abstract

Springback after unloading is an issue that directly reduces the accuracy of bent tubes, especially for Ti-alloy tubes which are of high strength and low Young's modulus. The Young's modulus, E ; wall thickness, t ; and neutral layer, D_e , of a tube vary during the bending process. These variations may influence the bending deformation of components, thus on springback. Considering these variations, an analytic elastic-plastic tube bending springback model was established in this study based on the static equilibrium condition. When these variations were considered individually or combinedly, the resulting springback angles were all larger and closer to the experimental results than the results when variations were not considered for a $D6 \text{ mm} \times t0.6 \text{ mm}$ Ti-3Al-2.5V Ti-alloy tube. The t variation contribution is the largest and decreases the prediction error by 41.2%-45.3%. D_e variation ranks second and decreases the error by 21.2%-25.3%. E variation is the least significant, decreasing the error by only 2.4%. Furthermore, the influence of the stable Young's modulus E_a on the springback is larger than the initial Young's modulus E_0 . Therefore, for the bending springback of tubes with a small difference between E_0 and E_a and under a normal bending radius, E variation effects can be neglected. While for tubes with large differences between E_0 and E_a , and high springback prediction requirements, the E variation should be replaced by E_a . The influences of the initial tube sizes, material properties and bent tube sizes of the Ti-3Al-2.5V tube on springback were obtained using the newly developed model.

Keywords: Springback; Analytic model; Tube bending; Young's modulus; Wall thickness; Neutral layer.

1. Introduction

When metal tubes undergo bending to form bent tubes, elastic-plastic deformation occurs. The elastic deformation will recover after unloading, i.e., springback will occur. The springback directly influences the precise form of the bent tube. When the springback value exceeds the permissible error, the geometric shape cannot satisfy the requirement, which significantly reduces the performance of the bent tube. This phenomenon is especially remarkable for tubes with high strength and low Young's modulus, such as Ti-alloy tubes. Thus, tube springback analyses after bending deformation have gained significant interest.

With the development of numerical simulation technology, the finite element method (FEM) has become one of most common methods used to analyze stainless steel, Al-alloy and Ti-alloy tube springback after bending. Via FE simulation, Murata et al. (2008) investigated the springback of Al-alloy and stainless steel tubes in the draw bending and press bending. They found that the hardening exponent had little effect on the springback. Paulsen and Welo (1996) conducted three-dimensional (3D) elastic-plastic finite element analyses (FEA) focused on the bending of Al-alloy profiles. They found that springback was influenced by the strain-hardening characteristic and the amount of axial loading, including that decreased strain hardening and increased tension reduced springback. Liao et al. (2014) performed FEA on twist springback prediction of asymmetric tube in rotary draw bending with different constitutive models. They found that the springback angle is sensitive to the hardening model. Xue et al. (2015) developed an FE model of mandrel rotary draw bending for accurate twist springback prediction of an asymmetric aluminium alloy tube. They found that the interfacial frictions have significant effects on twist springback of the tube. Through FE simulations, Zhan et al. (2014) found that Young's modulus variations had no effect on the variations trends of springback angles or the springback radius with the bending angle of Ti-alloy tubes. However, it did cause the values increase. Gu et al. (2008) established an FE model for the numerical controlled (NC) bending of thin-walled Al-alloy tubes and obtained the effects of geometry, materials and process parameters on springback. The results showed that the springback angle increases with the relative bending radius and Poisson ratio. Jiang et al. (2010b) developed an FE model for simulating the entire bending and springback process of a Ti-3Al-2.5V tube. Using the model, Jiang et al. (2010a) revealed the coupling effects of the bending angle and material properties on the springback angle of the Ti-3Al-2.5V tube. They found that, regardless of the bending angle, the Young's modulus, strength coefficient and hardening exponent have significant effect on the springback angle. Huang et al. (2015) embedded the variation law of the

contractile strain ratio (CSR) with deformation into the FE simulation for the NC bending of Ti-3Al-2.5V tubes. Through considering this CSR variation, Zhan et al. (2015) found that the prediction accuracy of the Ti-3Al-2.5V tube springback angles can be improved.

Considering that theoretical analysis can quickly solve for the springback and reflect the associated mechanism, law and major influence factors, it is important to analyze tube bending springback using analytic methods. In recent years, multiple analytic models have been developed to predict tube bending springback based on the classical springback theory, in which the springback bending moment and the bending moment are assumed equal in quantity and opposite in direction. Based on the classical springback theory, Al-Qureshi and Russo (2002) derived an analytic formula for predicting springback and residual stress distributions of thin-walled aluminum tubes. However, in their study, the material was presumed to be elastic-perfectly plastic, which does not reflect the response of metal tubes during bending deformation. Thus, to improve tube bending springback prediction accuracy, analytic models have been derived by assuming the material to be elastic-plastic hardening material. Megharbel et al. (2008) modified Al-Qureshi's model by assuming the material to be elastic-exponent hardening plastic material. Based on the classic springback theory, Li et al. (2012) deduced a springback equation by assuming the material to be an exponent hardening plastic material and considered neutral layer variation (or offset) effects. However, the elastic deformation was neglected in their analysis. In addition, making use of the triangle similarity relation of the tangential deformation during tube bending loading and unloading, E et al. (2009b) deduced a calculation formula for a 1Cr18Ni9Ti tube bending springback. They found that the springback angle decreases with the plastic modulus and relative wall thickness, but increases with the hardening exponent and Young's modulus.

As commonly known, the wall thickness and neutral layer vary with tube bending deformation. Using an FEA on NC bending of two Ti-3Al-2.5V tubes with outside diameters of 8 mm and 14 mm, respectively, under various normal bending radii, Jiang et al. (2011) discovered that the wall thicknesses along the crest lines of two bent tubes both resemble plateaus when the bending angle exceeds the critical angle. The maximum thinning reached 7% and 12.5% for the 8 mm and 14 mm tubes, respectively, and the maximum thickening reached 11% and 16% for both tubes, respectively. Through theoretical analyses, Tang (2000) considered that the neutral layer should move toward the bending center to balance the moment of the internal force because the outer wall is thinner than the

inner wall during pure tube bending. E et al. (2009a) found that the amount of neutral layer movement is inversely proportional to the relative bending radius based on theoretical analyses. Stachowicz (2000) found that the neutral layer of a copper elbow shifts outwards the bending center when the stress pattern is asymmetric by the theoretical analysis. Through 3D numerical analysis for a torque superposed spatial bending (TSSB) of high strength steel square profiles, Hudovernik et al. (2013) also found that there exists stress neutral layer shifts outwards the bending center. In recent years, the Young's modulus of tubes has been observed to vary with the deformation level. Through repeated loading-unloading experiments, Zhan et al. (2014) found that the Young's modulus of Ti-3Al-2.5V tubes rapidly decreased in the initial stage, then slowly decreased until stabilizing in the final stage. The variation can be approximately expressed as an exponential model. These Young's modulus, wall thickness and neutral layer variations influence bending deformation and springback of components. However, most existing analytic tube bending springback models did not consider these variations. Furthermore, most existing analytic tube bending springback models are based on the classical springback theory, where the springback bending moment and the bending moment are assumed equal in quantity and opposite in direction. However, for a bent tube undergoing an elastic-plastic deformation, after unloading, residual deformation, residual stress and residual bending moment still exist. This means that the springback bending moment should not equal the bending moment, which no longer meets the unloading principle of the classical springback theory. Therefore, an analytic springback model was derived in this study based on the static equilibrium condition and the deformation compatibility of deformation and aimed at improving the accuracy of tube bending springback predictions. In the model, the material was assumed to be an elastic-plastic hardening material and Young's modulus, wall thickness and neutral layer variations were considered. This model was evaluated by investigating the contributions of Young's modulus, wall thickness and neutral layer variations to the springback of a Ti-3Al-2.5V Ti-alloy tube. Then, the model was compared to existing springback analytic models and experimental results. Finally, the model was used to determine the influencing laws of various springback factors on the Ti-alloy tube.

2. Theoretical basis

2.1 Fundamental assumptions

Deformation processes are extremely complicated during tube bending and springback. The following assumptions are given to develop a springback prediction model for tube bending:

(1) The tube material is continuous and exhibits elastic-plastic and exponent-hardening behaviors, which satisfy the stress-strain relationship showing in Eq. (1).

$$\sigma = \begin{cases} E\varepsilon, & \text{when } \sigma \leq \sigma_s \text{ or } \varepsilon \leq \varepsilon_s \\ K(\varepsilon+b)^n, & \text{when } \sigma > \sigma_s \text{ or } \varepsilon > \varepsilon_s \end{cases} \quad (1)$$

where E is Young's modulus, K is strength coefficient, n is hardening exponent, b is a constant, σ is the flow stress, ε is strain, σ_s is the yielding stress, ε_s is the yielding strain and at yielding point $E\varepsilon_s = K(\varepsilon_s + b)^n$.

The Young's modulus variation with deformation is assumed to be a function of equivalent strain during elastic-plastic tube bending, as shown in Eq. (2).

$$E = \begin{cases} E_0, & \sigma \leq \sigma_s \\ E_\mu, & \sigma > \sigma_s \end{cases} \quad (2)$$

where E_0 is initial Young's modulus and E_μ is the Young's modulus relative to plastic deformation in the current moment, which can be expressed as Eq. (3) (Chatti and Hermi, 2011 and Zhan et al., 2014).

$$E_\mu = E_0 - (E_0 - E_a)(1 - e^{-\xi \bar{\varepsilon}}) \quad (3)$$

where ξ is a mechanical parameter that determines the rate of decrease of E_μ , $\bar{\varepsilon}$ is the equivalent strain and E_a is the stable Young's modulus for an infinitely large equivalent strain in Eq. (3).

(2) The shear stress, shear strain, thickness stress and circumferential deformation are ignored during tube bending and springback, which can be expressed by Eq. (4).

$$\begin{cases} \sigma_{ij} = 0 & (i \neq j) \\ \varepsilon_{ij} = 0 & (i \neq j) \\ \sigma_t = 0 \\ \varepsilon_D = 0 \end{cases} \quad (4)$$

where σ_{ij} ($i \neq j$), ε_{ij} ($i \neq j$), σ_t and ε_D represent the shear stress, shear strain, thickness stress and circumferential strain, respectively.

(3) The tube is isotropic and Bauchinger effects are ignored.

(4) The arbitrary cross-section of the tube remains plane before and after bending.

(5) The stress neutral layer always coincides with the strain neutral layer during the bending process.

(6) The volume is constant during the bending process, which can be written as Eq. (5).

$$\varepsilon_x + \varepsilon_y + \varepsilon_z = 0 \quad (5)$$

where $\varepsilon_x, \varepsilon_y, \varepsilon_z$ represent the three normal strain components.

(7) The friction between the dies and tube is neglected during the bending process.

(8) The inside radius of the tube, r , is considered constant because there is a mandrel inside the tube during the bending process.

(9) The flattening during tube bending was neglected.

2.2 Mechanical basis

(1) The balance differential equation and deformation equation compatibility

The material deformation obeys the balance differential equation (Eq. (6)) and deformation equation compatibility (Eq. (7)).

$$\begin{cases} \frac{\partial \sigma_x}{\partial x} + \frac{\partial \tau_{yx}}{\partial y} + \frac{\partial \tau_{zx}}{\partial z} = 0 \\ \frac{\partial \tau_{xy}}{\partial x} + \frac{\partial \sigma_y}{\partial y} + \frac{\partial \tau_{zy}}{\partial z} = 0 \\ \frac{\partial \tau_{xz}}{\partial x} + \frac{\partial \tau_{yz}}{\partial y} + \frac{\partial \sigma_z}{\partial z} = 0 \end{cases} \quad (6)$$

where σ_x, σ_y and σ_z are three normal stress components and $\tau_{yx}, \tau_{zx}, \tau_{xy}, \tau_{zy}, \tau_{xz}, \tau_{yz}$ are the six shear stress components.

$$\begin{cases} \varepsilon_x = \frac{\partial u}{\partial x} & \gamma_{xy} = \gamma_{yx} = \frac{1}{2} \left(\frac{\partial u}{\partial y} + \frac{\partial v}{\partial x} \right) \\ \varepsilon_y = \frac{\partial v}{\partial y} & \gamma_{yz} = \gamma_{zy} = \frac{1}{2} \left(\frac{\partial v}{\partial z} + \frac{\partial w}{\partial y} \right) \\ \varepsilon_z = \frac{\partial w}{\partial z} & \gamma_{zx} = \gamma_{xz} = \frac{1}{2} \left(\frac{\partial w}{\partial x} + \frac{\partial u}{\partial z} \right) \end{cases} \quad (7)$$

where $\gamma_{yx}, \gamma_{zx}, \gamma_{xy}, \gamma_{zy}, \gamma_{xz}, \gamma_{yz}$ are the six shear strain components and u, v and w are the three displacement components.

(2) Generalized Hooke's law

When the material undergoes elastic deformation, its stress-strain relationship follows the elastic generalized Hooke's law, which can be written as Eq. (8).

$$\begin{cases} \varepsilon_x = \frac{1}{E_0} [\sigma_x - \nu(\sigma_y + \sigma_z)] \\ \varepsilon_y = \frac{1}{E_0} [\sigma_y - \nu(\sigma_x + \sigma_z)] \\ \varepsilon_z = \frac{1}{E_0} [\sigma_z - \nu(\sigma_x + \sigma_y)] \end{cases} \quad (8)$$

where ν is Poisson ratio.

(3) Total strain theory

When the material undergoes plastic deformation, it's volume is invariant, and the material obeys the **Hencky total strain theory containing the elastic strain (Hencky, H., 1924)**, as shown in Eq. (9).

$$\begin{cases} \varepsilon_x = \left(\frac{1}{E'} + \frac{1}{3G} \right) \left[\sigma_x - \frac{1}{2}(\sigma_y + \sigma_z) \right] \\ \varepsilon_y = \left(\frac{1}{E'} + \frac{1}{3G} \right) \left[\sigma_y - \frac{1}{2}(\sigma_x + \sigma_z) \right] \\ \varepsilon_z = \left(\frac{1}{E'} + \frac{1}{3G} \right) \left[\sigma_z - \frac{1}{2}(\sigma_x + \sigma_y) \right] \end{cases} \quad (9)$$

where E' and G are plastic modulus and shear modulus, respectively.

(4) Equivalent stress and equivalent strain

The equivalent stress and equivalent strain can be obtained by Eqs. (10) and (11), respectively.

$$\bar{\sigma} = \frac{1}{\sqrt{2}} \sqrt{(\sigma_1 - \sigma_2)^2 + (\sigma_2 - \sigma_3)^2 + (\sigma_3 - \sigma_1)^2} \quad (10)$$

$$\bar{\varepsilon} = \frac{\sqrt{2}}{3} \sqrt{(\varepsilon_1 - \varepsilon_2)^2 + (\varepsilon_2 - \varepsilon_3)^2 + (\varepsilon_3 - \varepsilon_1)^2} \quad (11)$$

where σ_1 , σ_2 and σ_3 are the three major stresses, respectively, and ε_1 , ε_2 and ε_3 are three major strains, respectively.

When the shear stress and strain are ignored during elastic-plastic bending, the major stress is equal to the normal stress, and the equivalent stress and strain formulas can be simplified as Eqs. (12) and (13), respectively.

$$\bar{\sigma} = \frac{1}{\sqrt{2}} \sqrt{(\sigma_x - \sigma_y)^2 + (\sigma_y - \sigma_z)^2 + (\sigma_z - \sigma_x)^2} \quad (12)$$

$$\bar{\varepsilon} = \frac{\sqrt{2}}{3} \sqrt{(\varepsilon_x - \varepsilon_y)^2 + (\varepsilon_y - \varepsilon_z)^2 + (\varepsilon_z - \varepsilon_x)^2} \quad (13)$$

(5) Yield condition

Tubes are assumed to be isotropic materials that obey the **von Mises yield criterion** (Eqs. (14) and (15)) when elastic-plastic deformation occurs.

$$f(\sigma'_{ij}) = J_2' = C \quad (14)$$

$$J_2' = \frac{1}{6} [(\sigma_1 - \sigma_2)^2 + (\sigma_2 - \sigma_3)^2 + (\sigma_3 - \sigma_1)^2] = \frac{1}{3} \sigma_s^2 \quad (15)$$

where J_2' is the second deviator stress tensor.

Combining Eq. (10) and Eq. (15), the yield equation can be written as Eq. (16).

$$\bar{\sigma} = \sigma_s \quad (16)$$

(6) Static equilibrium condition

When the bent tube reaches a static equilibrium state after springback, the sum of axial forces on the tube cross-section is zero, as shown in Eq. (17).

$$F_\theta = 0 \quad (17)$$

3. Development of a tube bending springback model

3.1 Proposal of a springback analysis method

The unloading principle of the classic springback theory states that the springback bending moment during unloading and the bending moment during loading are equal in quantity and opposite in direction. During the elastic bending process, tube bending deformation will completely recover after unloading and the residual deformation is zero. Thus, the springback bending moment and the bending moment are equal in quantity and opposite in direction, which matches the classical springback theory unloading principle. However, for a tube undergoes an elastic-plastic bending, the deformation includes elastic deformation and plastic deformation. After unloading, residual deformation and residual stress exist (Jiang et al., 2010b), which means that a residual bending moment still exists. Therefore, the value of the springback bending moment should not be equal to the bending moment. This means that it no longer meets the classical springback theory unloading principle.

Therefore, this study proposes an elastic-plastic bending springback analysis based on the static equilibrium condition, where the residual stress and residual bending moment are allowed to exist after springback while they meet the static equilibrium condition. According to the condition, the sum of the residual stress after the springback is zero, for which an analytic tube bending springback model can be obtained. In the model, Young's modulus, wall thickness and neutral layer variations with deformation were incorporated to improve prediction accuracy.

3.2 Development of an analytic tube bending springback model

For a tube experiencing external loading, the wall thickness of the outer arc area becomes thinner and the wall thickness of inner arc area becomes thicker due to tensile and compressive deformation in these two zones, respectively. A strain neutral layer exists between the outside tensile deformation and

the inside compressive deformation of the tube. The strain neutral layer slightly offset toward the bending center from the geometrical neutral layer (D_e in Fig. 1) because the stress pattern is asymmetric (Stachowicz, 2000). Thus, it balances the force moments of the inside and outside deformations during the bending process.

Elastic deformation occurs first during external loading. As the external loading increases, deformation increases. During the process, the outermost and innermost materials reach a yield limit. They then undergo plastic deformation. The closer to the neutral layer, the less plastic deformation occurs. Certain material near the neutral layer experiences elastic deformation during the entire bending process. Thus, the bent tube cross-section can be divided into two elastic deformation zones and two plastic deformation zones, as shown in Fig. 1, including an outside elastic deformation zone, an outside plastic deformation zone, an inside elastic deformation zone and an inside plastic deformation zone. In Fig. 1, he_1 is the distance from the parting line of the outside elastic deformation zone and the outside plastic deformation zone to the geometrical neutral layer, with a position angle of α . he_2 is the distance from the parting line of the inside elastic deformation zone and the inside plastic deformation zone to the geometrical neutral layer, with a position angle of β .

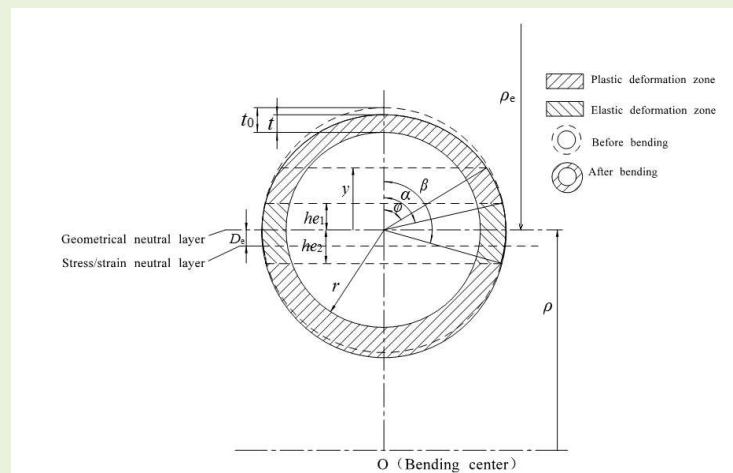


Fig. 1 The bent tube cross-section.

3.2.1 Stress during the tube bending process

In the elastic deformation zone, the stress-strain relationship of material obeys the general Hooke's law (Eq. (18)).

$$\begin{cases} \varepsilon_{\theta} = \frac{1}{E_0}(\sigma_{\theta} - \nu\sigma_D) \\ \varepsilon_D = \frac{1}{E_0}(\sigma_D - \nu\sigma_{\theta}) \\ \varepsilon_t = \frac{1}{E_0}[-\nu(\sigma_{\theta} + \sigma_D)] \end{cases} \quad (18)$$

where σ_{θ} and σ_D are the axial stress and the circumferential stress, respectively, and ε_{θ} and ε_t are the axial strain and thickness strain, respectively.

According to Eqs. (4) and (18), the axial stress-strain equation in the elastic deformation zone can be written as Eq. (19).

$$\sigma_{\theta} = \frac{E_0}{1-\nu^2} \varepsilon_{\theta} \quad (19)$$

In the plastic deformation zone, the stress-strain equation can be written as Eq. (20), according to the **Hencky total strain theory containing the elastic strain (Hencky, H., 1924)**.

$$\begin{cases} \varepsilon_{\theta} = \left(\frac{d\bar{\varepsilon}}{d\bar{\sigma}} + \frac{1}{3G} \right) \left(\sigma_{\theta} - \frac{1}{2}\sigma_D \right) \\ \varepsilon_D = \left(\frac{d\bar{\varepsilon}}{d\bar{\sigma}} + \frac{1}{3G} \right) \left(\sigma_D - \frac{1}{2}\sigma_{\theta} \right) \\ \varepsilon_t = \left(\frac{d\bar{\varepsilon}}{d\bar{\sigma}} + \frac{1}{3G} \right) \left[-\frac{1}{2}(\sigma_{\theta} + \sigma_D) \right] \end{cases} \quad (20)$$

According to Eqs. (4) and (20), Eq. (21) can be obtained.

$$\sigma_D = \frac{\sigma_{\theta}}{2} \quad (21)$$

According to Eqs. (4) and (5), the relationship between the axial and thickness strain in the plastic deformation zone can be written as Eq. (22).

$$\varepsilon_t = -\varepsilon_{\theta} \quad (22)$$

According to Eqs. (12), (13), (21) and (22), the equivalent stress and equivalent strain can be written as Eqs. (23) and (24), respectively.

$$\bar{\sigma} = \frac{1}{\sqrt{2}} \sqrt{\sigma_{\theta}^2 + \sigma_D^2 + (\sigma_{\theta} - \sigma_D)^2} = \frac{\sqrt{3}}{2} |\sigma_{\theta}| \quad (23)$$

$$\bar{\varepsilon} = \frac{2}{\sqrt{3}} |\varepsilon_{\theta}| \quad (24)$$

According to Eqs. (1), (23) and (24), the axial stress-strain relationship of the plastic deformation

zone during the tube bending process can be written as Eq. (25).

$$|\sigma_\theta| = \frac{2}{\sqrt{3}} \bar{\sigma} = \frac{2K}{\sqrt{3}} \left(\frac{2}{\sqrt{3}} |\varepsilon_\theta| + b \right)^n \quad (25)$$

The neutral layer variation (or offset) can be determined via Eq. (26), according to assumption (5) in Section 2.1 and the results of E et al. (2009a).

$$D_e = \rho - r \sqrt{(\rho/r)^2 - 1} \quad (26)$$

According to the definition of strain, the thickness strain and axial strain on a bent tube cross-section can be expressed as Eqs. (27) and (28), respectively, when considering the neutral layer variation (or offset).

$$\varepsilon_t = \ln \frac{t}{t_0} \quad (27)$$

$$\varepsilon_\theta = \ln \frac{\rho + y}{\rho - D_e} \quad (28)$$

In Eqs. (26)-(28) and Fig. 1, D_e is the stress and strain neutral layer variation/offset, r is the inside tube radius, t_0 is the initial tube wall thickness, t is the tube wall thickness after bending, ρ is the bending radius before springback and y is the distance between the measured position and the geometric neutral layer, which can be written as Eq. (29).

$$y = (r + t) \cos \varphi \quad (29)$$

where φ is the position angle of the tube cross-section, as shown in Fig. 1.

By substituting Eqs. (27)-(29) into Eq. (22), the tube wall thickness after bending can be deduced as Eq. (30).

$$t = \begin{cases} \frac{(\rho - D_e)t_0}{\rho}, & \varphi = \frac{\pi}{2} \\ \frac{-(\rho + r \cos \varphi) + \sqrt{(\rho + r \cos \varphi)^2 + 4 \cos \varphi t_0 (\rho - D_e)}}{2 \cos \varphi}, & \varphi \neq \frac{\pi}{2} \end{cases} \quad (30)$$

From Eqs. (24) and (28), the axial strain between the elastic deformation zone and the plastic deformation zone at the outside portion of the tube cross-section can be written as Eq. (31) since where yielding occurs.

$$\varepsilon_s = \bar{\varepsilon}_\alpha = \frac{2}{\sqrt{3}} \varepsilon_\alpha = \frac{2}{\sqrt{3}} \ln \frac{\rho + h e_1}{\rho - D_e} \quad (31)$$

According to Eq. (31), he_1 can be expressed as Eq. (32).

$$he_1 = (\rho - D_e) e^{\frac{\sqrt{3}}{2}\varepsilon_s} - \rho \quad (32)$$

From Fig. 1, Eq. (33) can be obtained.

$$y_\alpha = he_1 = (r + t_\alpha) \cos \alpha \quad (33)$$

According to Eq. (30), t_α can be expressed as Eq. (34).

$$t_\alpha = \frac{-(\rho + r \cos \alpha) + \sqrt{(\rho + r \cos \alpha)^2 + 4 \cos \alpha t_0 (\rho - D_e)}}{2 \cos \alpha} \quad (34)$$

By substituting Eqs. (32) and (34) into Eq. (33), α can be deduced as Eq. (35).

$$\alpha = \arccos \frac{\left[(\rho - D_e) e^{\frac{\sqrt{3}}{2}\varepsilon_s} - \rho \right] e^{\frac{\sqrt{3}}{2}\varepsilon_s}}{r e^{\frac{\sqrt{3}}{2}\varepsilon_s} + t_0} \quad (35)$$

Using the same procedures that produced he_1 and α , he_2 and β can be determined via Eqs.

(36) and (37), respectively.

$$he_2 = \rho - (\rho - D_e) e^{-\frac{\sqrt{3}}{2}\varepsilon_s} \quad (36)$$

$$\beta = \arccos \frac{\left[(\rho - D_e) e^{-\frac{\sqrt{3}}{2}\varepsilon_s} - \rho \right] e^{-\frac{\sqrt{3}}{2}\varepsilon_s}}{r e^{-\frac{\sqrt{3}}{2}\varepsilon_s} + t_0} \quad (37)$$

From Eqs. (19), (25), (35) and (37), the axial stress on the bent tube cross-section can be expressed by Eq. (38).

$$\sigma_\theta = \begin{cases} \frac{2K}{\sqrt{3}} \left(\frac{2}{\sqrt{3}} \varepsilon_\theta + b \right)^n, & 0 \leq \varphi \leq \alpha \\ \frac{E_0}{1-\nu^2} \varepsilon_\theta, & \alpha \leq \varphi \leq \beta \\ -\frac{2K}{\sqrt{3}} \left(-\frac{2}{\sqrt{3}} \varepsilon_\theta + b \right)^n, & \beta \leq \varphi \leq \pi \end{cases} \quad (38)$$

3.2.2 Residual stress after springback

The residual axial stress, σ_θ^r , after springback can be expressed as Eq. (39).

$$\sigma_\theta^r = \sigma_\theta + \Delta \sigma_\theta \quad (39)$$

where $\Delta \sigma_\theta$ is the axial stress during springback. Assuming that the deformation during the springback

process is completely elastic deformation (Al-Qureshi, 1999), the axial stress during springback can be obtained by Eq. (40), according to Eq. (19).

$$\Delta\sigma_{\theta} = \frac{E}{1-\nu^2} \Delta\varepsilon_{\theta} = \frac{E}{1-\nu^2} \ln\left(\frac{\rho_e - y}{\rho_e + D_e}\right) \quad (40)$$

where $\Delta\varepsilon_{\theta}$ is the axial strain during springback, ρ_e is the springback radius (Fig. 1) and $\ln\left(\frac{\rho_e - y}{\rho_e + D_e}\right)$ can be simplified to $\frac{-y - D_e}{\rho_e + D_e}$ because the axial strain during springback is very small.

From Eqs. (2) and (38)-(40), the residual axial stress distribution on the cross-section after springback can be written as Eq. (41).

$$\sigma_{\theta}^r = \begin{cases} \frac{2K}{\sqrt{3}} \left(\frac{2}{\sqrt{3}} \varepsilon_{\theta} + b\right)^n + \frac{E_u}{1-\nu^2} \frac{-y - D_e}{\rho_e + D_e}, & 0 \leq \varphi \leq \alpha \\ \frac{E_0}{1-\nu^2} \left(\varepsilon_{\theta} + \frac{-y - D_e}{\rho_e + D_e}\right), & \alpha < \varphi < \beta \\ -\frac{2K}{\sqrt{3}} \left(-\frac{2}{\sqrt{3}} \varepsilon_{\theta} + b\right)^n + \frac{E_u}{1-\nu^2} \frac{-y - D_e}{\rho_e + D_e}, & \beta \leq \varphi \leq \pi \end{cases} \quad (41)$$

3.2.3 Springback model

According to the static equilibrium condition (Eq. (17)), the sum of the residual axial stress after springback should equal zero (Eq. (42)).

$$F_{\theta} = \int_0^{\pi} \sigma_{\theta}^r (t^2 + 2rt) d_{\varphi} = 0 \quad (42)$$

From Eqs. (41) and (42), Eqs. (43) and (43.1) can be obtained.

$$\frac{1}{\rho_e + D_e} = \frac{C_1 + C_2 + C_3}{C_4 + C_5 + C_6} \quad (43)$$

$$\left\{ \begin{array}{l} C_1 = \int_0^{\alpha} \frac{2KM}{\sqrt{3}} \left(\frac{2}{\sqrt{3}} \varepsilon_{\theta} + b\right)^n d_{\varphi} \\ C_2 = \int_{\alpha}^{\beta} \frac{E_0 M}{1-\nu^2} \varepsilon_{\theta} d_{\varphi} \\ C_3 = \int_{\beta}^{\pi} -\frac{2KM}{\sqrt{3}} \left(-\frac{2}{\sqrt{3}} \varepsilon_{\theta} + b\right)^n d_{\varphi} \\ C_4 = \int_0^{\alpha} \frac{E_{\mu} M (y + D_e)}{1-\nu^2} d_{\varphi} \\ C_5 = \int_{\alpha}^{\beta} \frac{E_0 M (y + D_e)}{1-\nu^2} d_{\varphi} \\ C_6 = \int_{\beta}^{\pi} \frac{E_{\mu} M (y + D_e)}{1-\nu^2} d_{\varphi} \end{array} \right. \quad (43.1)$$

where C_1 is the sum of the axial forces in the outside plastic deformation zone before springback, C_2 is the sum of the axial forces in the outside and inside elastic deformation zones before springback, C_3 is the sum of the axial forces in the inside plastic deformation zone before springback, C_4 is $-(\rho_e + D_e)$ times the sum of the axial forces in the outside plastic deformation zone during springback, C_5 is $-(\rho_e + D_e)$ times the sum of the axial forces in the outside and inside elastic deformation zones during springback, C_6 is $-(\rho_e + D_e)$ times the sum of the axial forces in the inside plastic deformation zone during springback and $\mathbf{M} = \mathbf{t}^2 + 2\mathbf{tr}$.

Thus, the residual curvature after springback can be obtained by Eq. (44).

$$\frac{1}{\rho_e^r} = \frac{1}{\rho - D_e} - \frac{1}{\rho_e + D_e} \quad (44)$$

Because the difference in tube fiber lengths before and after springback is minor, they can be assumed equal (Eq. (45)).

$$(\rho - D_e)\theta = \rho_e^r \theta^r \quad (45)$$

where θ^r is the bending angle after springback.

From Eqs. (44) and (45), the springback angle can be obtained as Eq. (46).

$$\Delta\theta = \theta - \theta^r = \frac{\rho - D_e}{\rho_e + D_e} \theta \quad (46)$$

3.2.4 Resolving for the springback angle

The springback angle is an implicit function of the position angle, φ , according to Eqs. (43), (43.1) and (46). Thus, it is difficult to explicitly express and directly resolve. Therefore, numerical integral methods can be used to resolve the values of C_1 - C_6 , allowing the tube springback angle after bending to be obtained. The detailed flow chart used to solve for the springback angle is shown in Fig. 2.

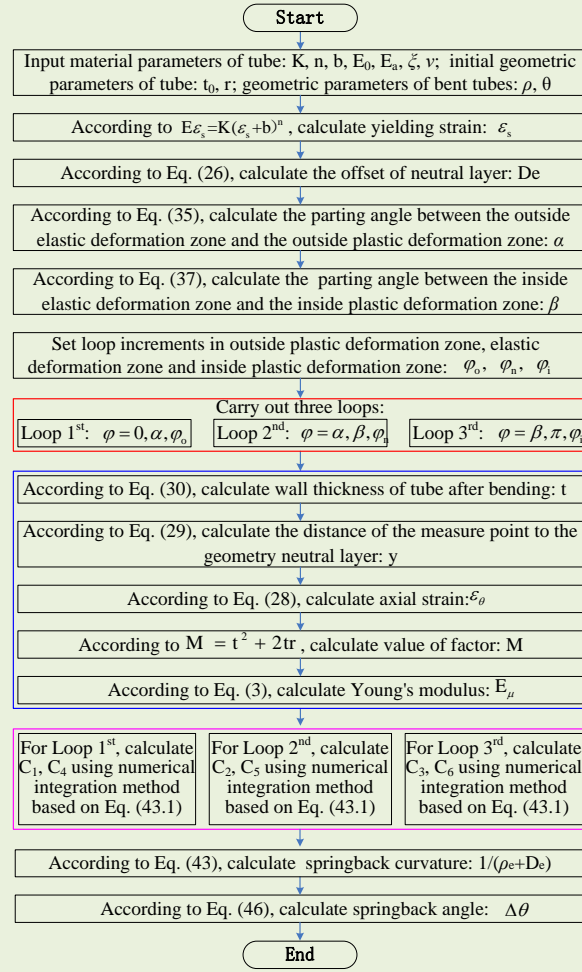


Fig. 2 Flow chart used to solve for the springback angle

4. Results and discussion

First, the analytic tube bending springback model developed in this study was evaluated based on the contributions of Young's modulus, wall thickness and neutral layer variations to the springback. Then, this model was testified via comparison with existing analytic models and experimental springback results. Furthermore, error sources relative to this model were analyzed. Finally, this model was applied to a tube bending to investigate the influence of the initial tube geometric shapes, tube material properties and bent tube geometric shapes.

In recent years, Ti-3Al-2.5V Ti-alloy tubes have been used frequently in fields of aeronautics and aerospace due to their advantages of high strength/weight ratio, excellent fatigue resistance and corrosion resistance, and good welding performance (Zhan et al., 2015). Therefore, two sizes of Ti-3Al-2.5V Ti-alloy tubes were analyzed in this study. One is a D6 mm × t0.6 mm tube with an initial outside diameter of 6 mm and wall thickness of 0.6 mm, while the other is a D12 mm × t0.9 mm tube with an initial outside diameter of 12 mm and wall thickness of 0.9 mm. The property parameters of

these two tubes were obtained via tensile testing, as shown in Table 1.

Table 1 Material property parameters of the tubes.

Parameters	E_0 /MPa	E_a /MPa	ξ	ν	K /MPa	n	b
D6 mm × t0.6 mm	97541	94215	-97.45	0.3	1038.9	0.093	-0.0040
D12 mm × t0.9 mm	100380	94109	-59.08	0.291	1326.5	0.070	-0.0006

The bending experiments for D6mm×t0.6mm Ti-3Al-2.5V tubes were conducted on an Eaton VB50 rotary bender, and the bending experiments for D12mm×t0.9mm Ti-3Al-2.5V tubes were conducted on a GQ W27YPC-63 rotary bender. The basic die composition for rotary tube bending is composed of a bending die, a clamping die, a wiper die, a pressure die, a cylindrical mandrel and several balls (or a cylindrical mandrel with a hemisphere head), as shown in Fig. 3. The die composition for bending the D6mm×t0.6mm Ti-3Al-2.5V tubes was composed of a bending die, a clamping die, a pressure die and a cylindrical mandrel with a hemisphere head. For the bending of the D12mm × t0.9mm Ti-3Al-2.5V tubes, a wiper die was applied, and the cylindrical mandrel with a hemisphere head was replaced by a cylindrical mandrel and a ball. During bending experiments, the lubricant among the tube, mandrel, ball, pressure die and wiper die is extrusion oil S980B. The bending parameters for these two kinds of tubes are shown in Table 2. The springback angle is the difference of bending angle before and after springback. After springback, the bending angle was measured by a universal bevel protractor.

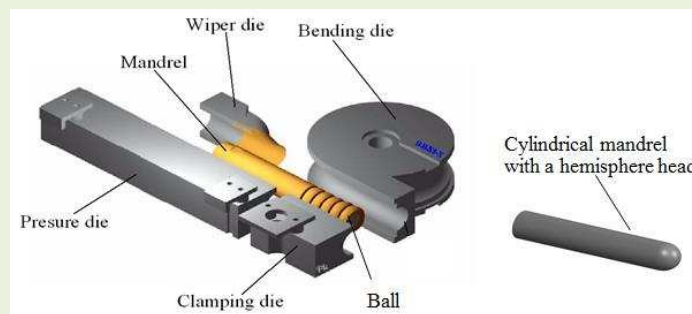


Fig. 3 Basic die composition for rotary tube bending.

Table 2 Bending parameters of Ti-3Al-2.5V tubes.

Parameters	D12mm×t0.9mm	D6mm×t0.6mm
Bending radius /mm	24	18
Mandrel feed /mm	1	1
Ball thickness /mm	5	-
Bending speed /rad/s	0.80	0.80
Boosting velocity /mm/s	19.2	14.4
Pushing ratio /%	100	100
Mandrel diameter /mm	9.94	4.64

4.1 Effect of Young's modulus, wall thickness and neutral layer variations

In this section, the contributions of Young's modulus, E , wall thickness, t , and neutral layer, D_e , variations to tube bending springback were studied by comparing springback angles of experiment and prediction obtained using the model in this study under various considerations about D_e , t and E for a $D6 \text{ mm} \times t0.6 \text{ mm} \times \rho18 \text{ mm}$ Ti-3Al-2.5V tube, as shown in Fig. 4. During the bending process, the bending radius was 18 mm (i.e., the relative bending radius $\rho/D=3$). Fig. 4 shows that the springback angle prediction errors of the model under various bending angles are different. Thus to easily evaluate the prediction capability of the analytic springback model in this study, an index named the average relative springback angle error at different bending angles (Eq. (47)) was proposed. Based on Eq. (47), the average relative springback angle errors under different considerations about D_e , t and E were calculated, as shown in Table 3.

$$\delta = \frac{1}{m_0} \sum_{i=1}^{m_0} \left| \frac{\Delta\theta_{ia} - \Delta\theta_{ie}}{\Delta\theta_{ie}} \right| \times 100 \quad (47)$$

where $\Delta\theta_{ia}$ represents the analytic springback angle value, $\Delta\theta_{ie}$ is the experimental springback angle value, δ is the average relative error and m_0 is the total data number of various bending angles.

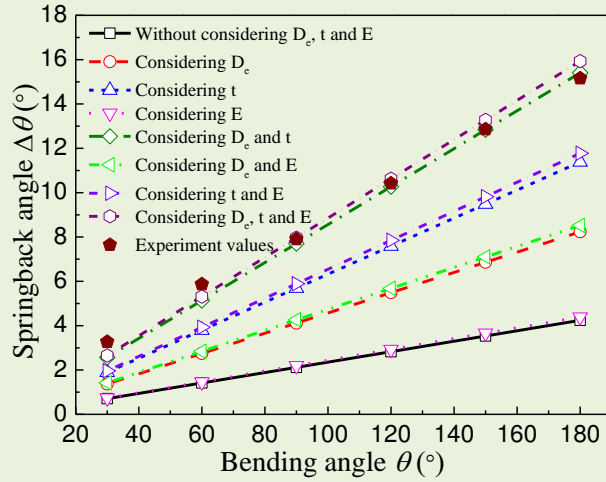


Fig. 4 Springback angles of experiment and prediction obtained using the model in this study under various considerations about D_e , t and E for a $D6 \text{ mm} \times t0.6 \text{ mm} \times \rho18 \text{ mm}$ Ti-3Al-2.5V tube.

Table 3 Average relative springback angle errors of analytic results from the model in this study and different considerations about D_e , t and E .

Considerations of D_e , t , and E	None	D_e	t	E	D_e and t	D_e and E	t and E	D_e , t and E
Average relative error (%)	74.0	49.5	30.1	73.0	6.6	47.7	27.7	6.5

Fig. 4 and **Table 3** illustrate that the springback angles at a given bending angle become larger and approach the experimental results when considering one, two or all three parameters than those without considering variations in E , t and D_e . The predicted springback angles are closest to the experimental results for the cases that consider t and D_e and that consider t , D_e and E .

Fig. 4 and **Table 3** also show that the springback angle significantly increases after introducing t variations, while D_e ranks second and E variations cause only a slight increase. **The last finding is in accordance with that from the previous finite element analysis on the bending of a $D6 \text{ mm} \times t0.5 \times \rho12 \text{ mm}$ Ti-3Al-2.5V tube (Zhan et al., 2014). Though except for the outside diameter, the conditions in these two cases, including wall thickness, the bending radius and material properties are different.** The springback angle prediction errors can be decreased by 43.9%, 24.5% and 1.0% under these three cases, respectively. This means that, when only one of three parameters was considered, the variation in t and E are the most and the least significant parameters affecting on springback, respectively.

As comparing to the springback angles without considering the variation in E , t , and D_e , the springback angle increases after introducing both t and D_e variations is the largest, while introducing t

and E variations ranks second and considering D_e and E variations ranks last. The springback angle prediction precisions can be improved by 67.4%, 46.3%, and 26.3% under these three cases, respectively. This means that, when the variations of two parameters were considered together, the comprehensive contribution of D_e and t is the largest, that of t and E is second and that of D_e and E is the least.

As comparing to the springback angles without considering the variation in t, D_e and E, there is a significant springback value increase when all three parameters are considered together, resulting in an average error decrease from 74.0% to 6.5%.

From Fig. 4 and Table 3, it can be noted that the springback values significantly increase when considering t variations versus without considering t variations, with average error decreases from 74.0% to 30.1% (decreased by 43.9%), from 73.0% to 27.7% (decreased by 45.3%), from 49.5% to 6.6% (decreased by 42.9%) and from 47.7% to 6.5% (decreased by 41.2%) when comparing the values considering t to those without considering t, E and D_e , considering both t and E to those only considering E, considering both t and D_e to those only considering D_e , considering t, D_e and E to those considering both D_e and E, respectively.

These springback angle differences are caused by the original uniform wall thickness becoming non-uniform, with decreasing thickness from the neutral layer to the outermost portion and increasing thickness from the neutral layer to the innermost portion (with the maximum thinning ratio and thickening ratio of about 15% and 20%, respectively, as shown in Fig. 5). This will result in axial strain (Fig. 6), axial stress (Fig. 7) and axial force (Fig. 8) variations under these conditions. As seen from Fig. 6, the t variations cause the axial strain to decrease before springback (Fig. 6a), increase during springback (Fig. 6b) and decrease after springback (Fig. 6c) by comparing the results considering t to those without considering t, E and D_e , considering both t and E to those only considering E, considering both t and D_e to those only considering D_e , considering t, D_e , E, and to those considering both D_e and E, respectively. These strain variations from t variations cause stress variations (Fig. 7). As Fig. 7b illustrates, the farther to the neutral layer, the larger the axial stress value during springback. Thus, it leads to significant differences in the axial stress values and distribution after springback (Fig. 7c) versus before springback (Fig. 7a). The axial stress after springback is smaller than before springback. In the zones farther from the neutral layer, the axial stress after springback becomes opposite of the axial stress before springback (Fig. 7a and c). As Figs. 7a, b and c illustrate, the t

variations cause a decrease in the axial stress before springback (Fig. 7a) and an increase in the axial tensile stress during and after springback (Figs. 7b and c). by comparing the results considering t to those without considering t , E and D_e , considering both t and E to those only considering E , considering both t and D_e to those only considering D_e , considering t , D_e , E , and to those considering both D_e and E , respectively. Introducing t variations will lead to a decrease in the area of the outside deformation zone and an increase in the area of the inside deformation zone. These stress and area variations from t variations cause the axial force to decrease in the outer plastic deformation zone before springback (C_1) (Fig. 8a) and during springback (C_4) (Fig. 8d), in the elastic deformation zone before springback (C_2) (Fig. 8b) and during springback (C_5) (Fig. 8e), and in the inside plastic deformation zone before springback (C_3) (Fig. 8c) and during springback (C_6) (Fig. 8f). Thus, the sums of the axial forces before springback (the sum of C_1 , C_2 and C_3 in Fig. 8g) and during springback both increase (the sum of C_4 , C_5 and C_6 in Fig. 8h), and the increased axial force ratio before springback are larger than during springback. This difference in ratios leads to an increase in the springback curvature according to Eq. (43) (Fig. 8i).

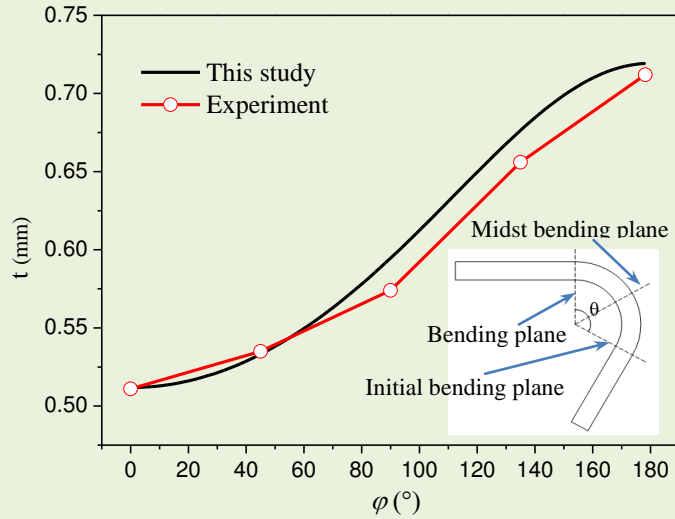
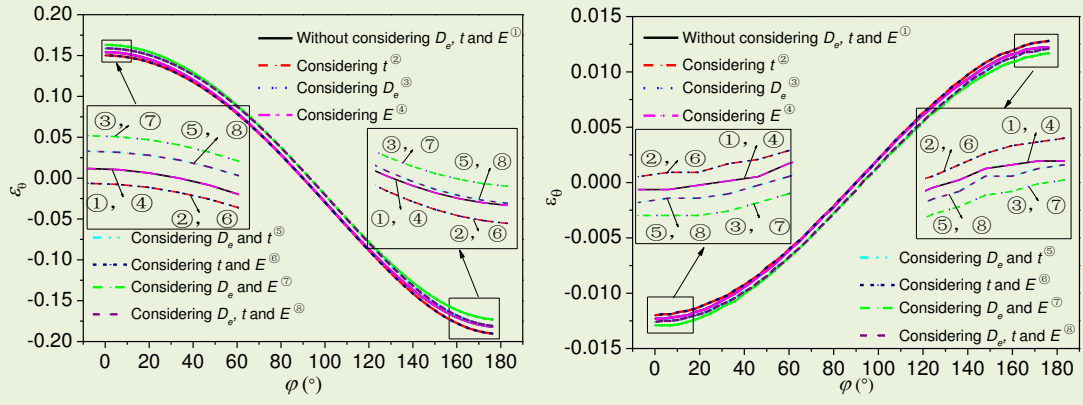
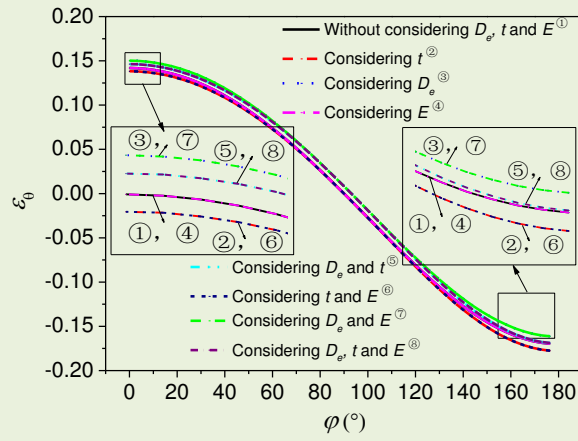


Fig. 5 Analytic and experimental thickness distribution along the midst bending plane of a D6 mm \times t0.6 mm \times ρ 18 mm Ti-3Al-2.5V bent tube with $\theta = 120^\circ$



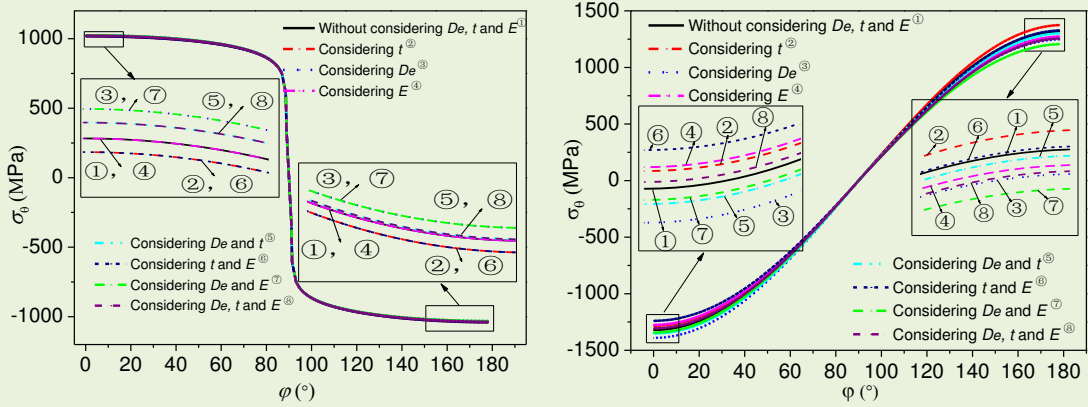
(a)

(b)



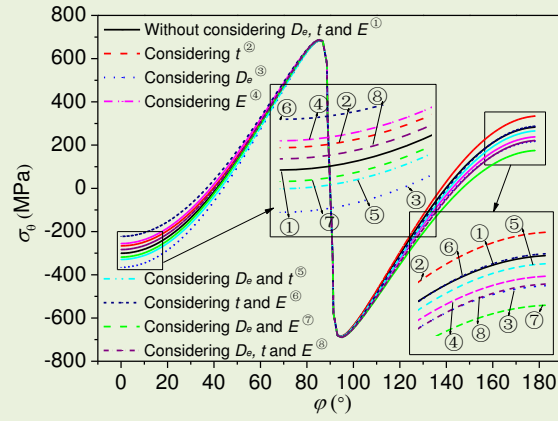
(c)

Fig. 6 Axial strain distributions before springback (a), during springback (b) and after springback (c) along a cross-section of a $D6 \text{ mm} \times t0.6 \text{ mm} \times \rho 18 \text{ mm}$ Ti-3Al-2.5V tube under various considerations about t , D_e and E .



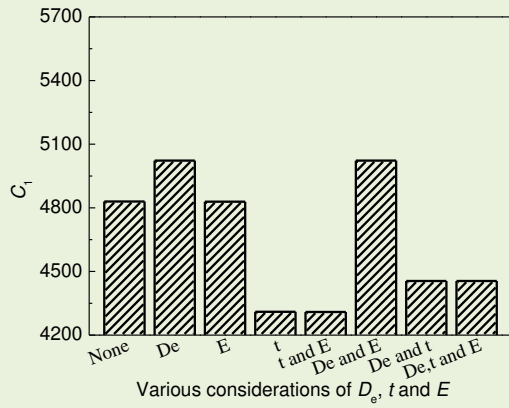
(a)

(b)

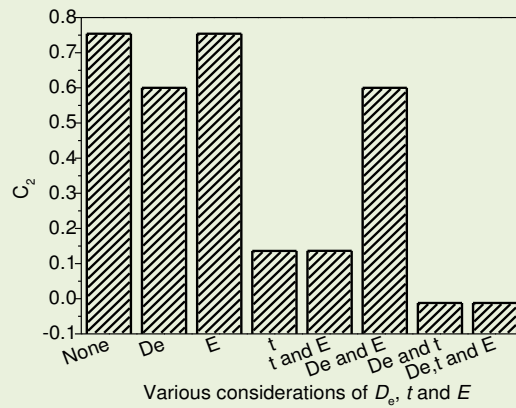


(c)

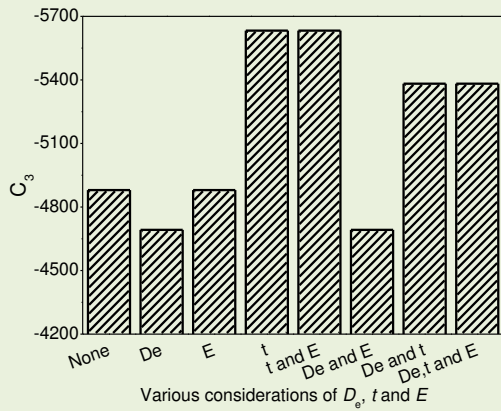
Fig. 7 Axial stress distributions before springback (a), during springback (b) and after springback (c) along a cross-section of a $D_6 \text{ mm} \times t 0.6 \text{ mm} \times \rho 18 \text{ mm}$ Ti-3Al-2.5V tube under various considerations about t , D_e and E .



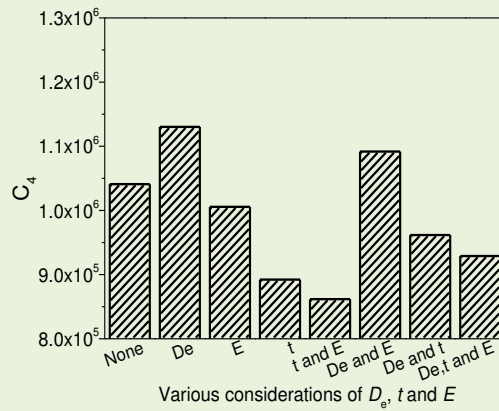
(a)



(b)



(c)



(d)

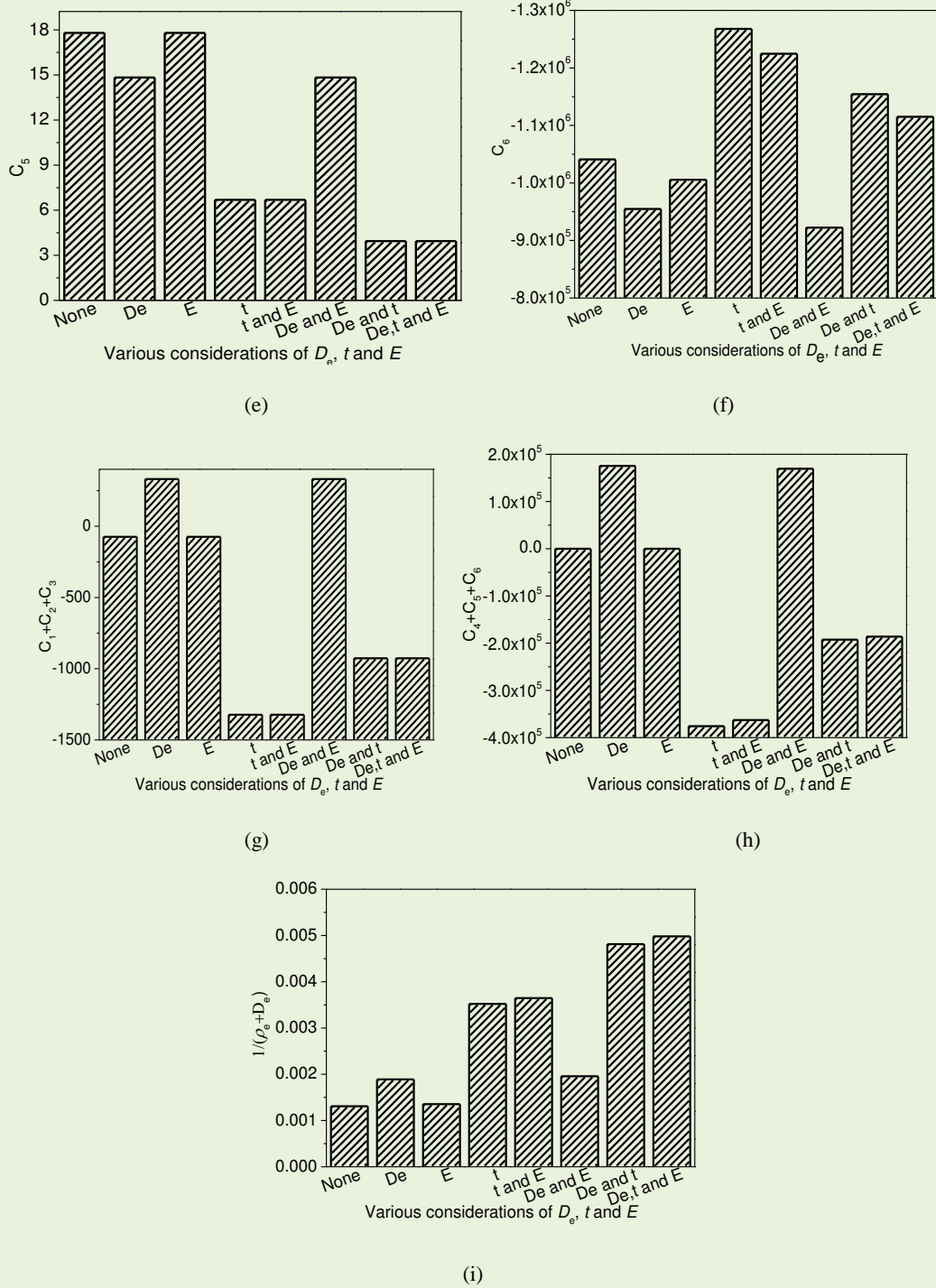


Fig. 8 Effect of various considerations of D_e , t and E on C_1 (a), C_2 (b), C_3 (c), C_4 (d), C_5 (e), C_6 (f), $C_1+C_2+C_3$ (g), $C_4+C_5+C_6$ (h) and $1/(\rho_e + D_e)$ (i).

Fig. 4 and Table 3 also illustrate that the springback values considering neutral layer variations are larger than those without this consideration, with average errors decrease from 74.0% to 49.5% (decreased by 24.5%), from 73.0% to 47.7% (decreased by 25.3%), from 30.1% to 6.6% (decreased by 23.5%) and from 27.7% to 6.5% (decreased by 21.2%), by comparing values considering D_e to those

without considering E , t and D_e , considering both D_e and E to those only considering E , considering both D_e and t to those only considering t and considering E , t and D_e to those considering both E and t , respectively.

These springback angle differences caused by different considerations about D_e are due to that the strain neutral layer, which will slightly offset toward the inside deformation zone, causes axial strain (Fig. 6), axial stress (Fig. 7) and axial force (Fig. 8) variations under these conditions. As seen from Fig. 6, the D_e variations cause an increase in the axial strain before springback (Fig. 6a), a decrease in the axial strain during springback (Fig. 6b) and an increase in the axial strain after springback (Fig. 6c), by comparing the results considering D_e to those without considering E , t and D_e , considering both D_e and E to those only considering E , considering both D_e and t to those only considering t , considering E , t and D_e to those considering both E and t , respectively. These strain variations cause an increase in the axial stress before springback (Fig. 7a) and a decrease in the axial stress during (Fig. 7b) and after springback (Fig. 7c). The introduction of neutral layer variations will lead to an increase in the area of the outside deformation zone and a decrease in the area of the inside deformation zone. These axial strain, axial stress and deformation zone area variations due to D_e variations exhibit an opposite trend as those caused by t variations. The stress and area variations caused by D_e variations lead to an increased axial force in the outside plastic deformation zone before springback (C_1) (Fig. 8a) and during springback (C_4) (Fig. 8d), a decrease in the elastic deformation zone before springback (C_2) (Fig. 8b) and during springback (C_5) (Fig. 8e) and a decrease in the inside plastic deformation zone before springback (C_3) (Fig. 8c) and during springback (C_6) (Fig. 8f). Thus, the sum of the axial forces increases from a negative value to a positive value before springback (the sum of C_1 , C_2 and C_3 in Fig. 8g) and also during springback (the sum of C_4 , C_5 and C_6 in Fig. 8h). In addition, the increased axial force ratio before springback is larger than during springback. This difference in ratios leads to a springback curvature increase based on Eq. (43) (Fig. 8i). Because the degree of variation in the sum of the axial forces (including $C_1+C_2+C_3$ and $C_4+C_5+C_6$) caused by D_e is significantly less than that caused by t , the springback considering D_e variations is smaller than considering t variations.

Furthermore, Fig. 4 and Table 3 illustrate that the springback angles considering E variations slightly increase when compared to those without considering E variations, with average errors decreasing from 74.0% to 73.0%, from 49.5% to 47.7%, from 30.1% to 27.7%, and from 6.6% to 6.5%, when comparing these values considering E to those without considering E , t and D_e , considering both

E and D_e to those only considering D_e , considering both E and t to those only considering t, considering E, t and D_e to those considering both D_e and t, respectively. These are a result of the Young's modulus distribution in the hoop direction of the tube (Fig. 9), and the variations in C_1 - C_6 when E variations are introduced (Fig. 8). As Fig. 9 showing, the Young's modulus near the neutral layer sharply increases from a stable value, E_a , to the initial value, E_0 , and remains unchanged in a very narrow zone. It then decreases to E_a , which is nearly equal to the stable E_a value in constant zones. This is because most of the zone along the cross-section underwent large plastic deformation after bending, and only the narrow zone near the neutral layer experienced elastic deformation. Thus, E variations have no influence on the bending deformation in any zone or the springback deformation within the elastic deformation zones. Therefore, no C_1 , C_2 , C_3 and C_5 (Figs. 8a-c and e) variations occur. In addition, only a slight decrease occurs in the unloading slope of the outside and inside plastic deformation zones, which is a result of the limited E variations within 3.4% from its initial value (97541 MPa) to its stable value (94215 MPa) for the tube, thus a little decreases in C_4 and C_6 (Figs. 8d and f), respectively. Thus, the springback angle slightly increases due to introducing E variations.

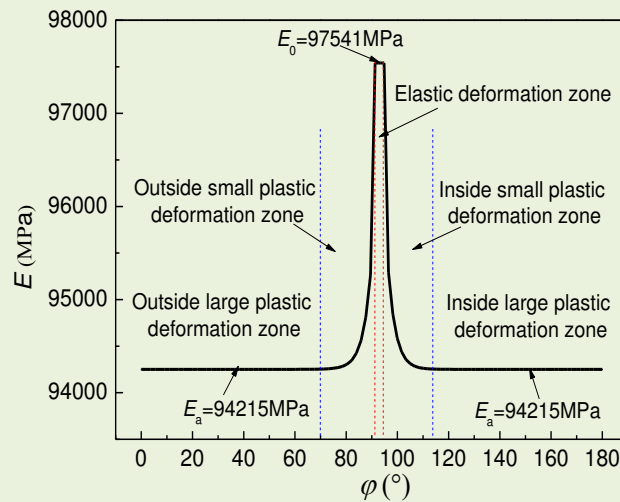


Fig. 9 Distribution of E along a cross-section of a D6 mm \times t0.6 mm \times ρ 18mm Ti-3Al-2.5V bent tube.

To further investigate the effect of Young's modulus on springback, tube springback angle variations with various initial Young's modulus and stable Young's modulus values were studied, as shown in Fig. 10. In Fig. 10, the reference value of initial Young's modulus and stable Young's modulus values are 97541 MPa and 94215 MPa, respectively, which are the same as those in Table 1. Because the initial Young's modulus value should be larger than its stable value, the initial Young's modulus floats 5%, 10%, 15% and 20% upward based on its reference value in Fig. 10a, while the stable Young's modulus floats 5%, 10%, 15% and 20% downward based on its reference value in Fig.

10b.

Fig. 10a illustrates that the initial Young's modulus has little influence on the springback. This is because the variation in E_0 only causes a variation in the unloading slope within the elastic deformation zone and the small plastic deformation zone, which account for a very small portion of the cross-section (Fig. 9). Fig. 10b shows that the springback angle increases as the stable Young's modulus decreases, and increase trend increases as the bending angle increases. This is because the decrease in E_a will cause a decrease in the unloading slope of the outside and inside plastic deformation zones (Fig. 9), thereby increasing the springback angle. Comparing Fig. 10a and Fig. 10b, it can be seen that the influence of E_a on the springback is more obvious than that of E_0 . This is because the range of the outside and inside large plastic deformation zones, which E_a affects, is larger a lot than the range of the elastic deformation zone and small plastic deformation zone, which E_0 affects.

This different effects between E_0 and E_a on springback means that the effects of the Young's modulus variations can be negligible for the springback of tubes with a small difference between E_0 and E_a and bent under a normal bending radius ($\rho/D=2-4$) (Jiang et al., 2011), where elastic deformation encompasses a very small portion of all deformation zones (Fig. 9). While for tubes with large differences between E_0 and E_a , if given high springback prediction requirements, the E variations should be replaced by the stable value of Young's modulus E_a since it affects most of deformation zones on cross-section.

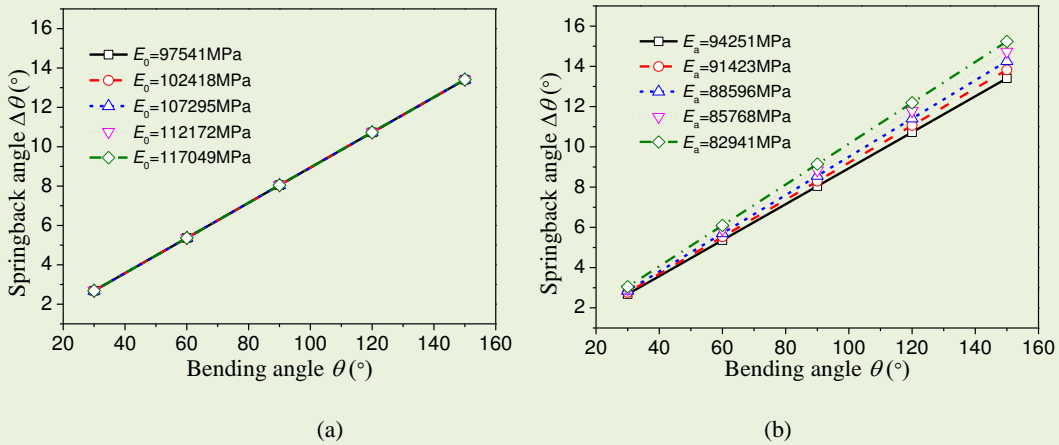


Fig. 10 Springback angle variations based on different initial Young's moduli (a) and stable Young's moduli (b).

4.2 Reliability evaluation

To evaluate the reliability of the analytic elastic-plastic tube bending springback model developed in this study, the springback results of $D6 \text{ mm} \times t0.6 \text{ mm} \times \rho18 \text{ mm}$ and $D12 \times t0.9\text{mm} \times \rho24 \text{ mm}$ Ti-3Al-2.5V Ti-alloy tubes after bending, while introducing t , D_e and E variations were examined

compared our model results to existing analytic model results (Al-Qureshi and Russo (2002), Megharbel et al. (2008), Li et al. (2012), and E et al. (2009b)), as shown in Fig. 11 and Table 4. The characteristics of these existing analytic models are listed in Table 5.

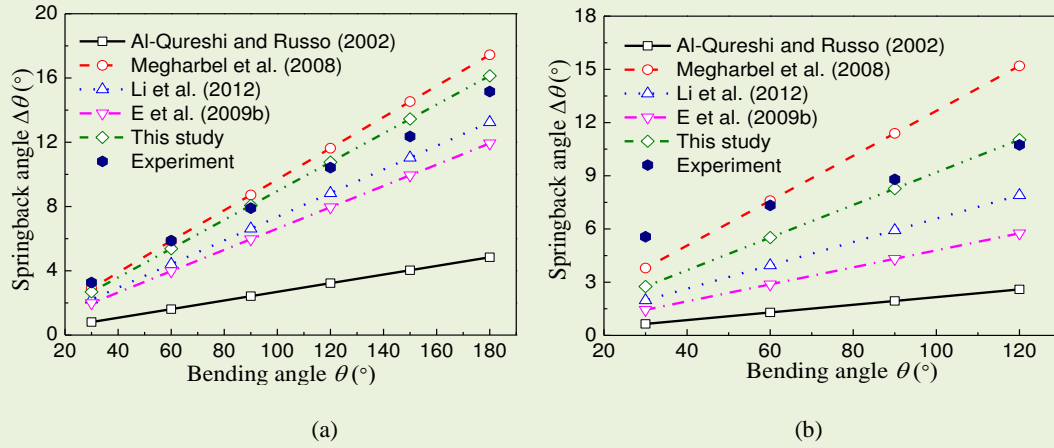


Fig. 11 Predicted and experimental springback angles: (a) D6 mm \times t0.6 mm (b) D12 mm \times t0.9 mm.

Table 4 Average relative springback errors of existing analytic models and the model in this study.

Ref.	Al-Qureshi and Russo (2002)	Megharbel et al. (2008)	Li et al. (2012)	E et al. (2009b)	This study
D6 mm \times t0.6 mm	70.3	11.0	18.7	26.7	6.5
D12 mm \times t0.9 mm	81.1	26.6	42.4	58.1	21.0

Table 5 Characteristics of existing analytic springback models.

Ref.	Material model	Principle of unloading springback	Similarities
Al-Qureshi and Russo (2002)	Elastic-perfectly plastic	Classical springback theory	Without considering the E , t , and D_e variations, except that Li et al. (2012) considered D_e variations
E et al. (2009b)	Exponent hardening plastic	Similarity in unloading triangle to elastic loading triangle	
Megharbel et al. (2008)	Elastic-exponent hardening plastic	Classical springback theory	
Li et al. (2012)	Exponent hardening plastic	Classical springback theory	

Fig. 11 illustrates that the springback angles predicted using these analytic models all increase nearly linearly as the bending angle increases. Based on the classic springback theory and when considering the tube material to be elastic-perfectly plastic, the springback angles predicted by Al-Qureshi and Russo (2002) are the lowest. When the tube material was considered to be exponent hardening, the Megharbel et al. (2008) prediction yielded the highest springback angle values. When the tube material was considered to be an exponent hardening material and neutral layer variations were introduced, Li et al. (2012) produced a value between the values of Al-Qureshi and Russo (2002) and Megharbel et al. (2008). The prediction line based on the similar triangle unloading theory, which

was predicted by E et al. (2009b), is the second lowest. The prediction line using the model developed in this study is the second highest. This is due to the classic springback theory assumed that the bending and unloading moments are equal, which will cause a large unloading moment leading to over-springback. The static equilibrium springback theory can avoid this over-springback because it accounts for the residual moment. The similar triangle unloading theory is an approximate method, where the unloading stress and strain are determined only through the outer surface stress, strain and similarity between the unloading triangle and elastic loading triangle. Furthermore, the elastic-perfectly plastic model will lead to under-springback due to neglecting the hardening effect. Accounting for wall thickness, neutral layer and Young's modulus variations will cause the springback to increase due to providing more accurate strain, stress and deformation zone area calculations. Additionally, neglecting the elastic deformation will also bring about inaccurate springback results.

Thus, comparing these predictions to the experimental results suggests that for both of the bent tubes, the prediction accuracy of the model developed in this study is the highest. The Megharbel et al. (2008) model ranks the second, the Li et al. (2012) model ranks third, the E et al. (2009b) model ranks fourth and the Al-Qureshi and Russo (2002) model ranks last. These comparisons show that the analytic elastic-plastic tube bending springback model, which is based on the static equilibrium condition and considers t , E and D_e variations is reliable.

4.3 Error analysis

The analysis in Section 4.2 shows that the springback prediction precision of the Ti-3Al-2.5V tubes was improved using the analytic model developed in this study. However, disparities still exist between the predicted and experimentally derived springback angles. The disparities for the $D6 \text{ mm} \times t0.6 \text{ mm} \times \rho18 \text{ mm}$ and $D12 \text{ mm} \times t0.9 \text{ mm} \times \rho24 \text{ mm}$ tubes are 6.5% and 21.0%, respectively.

The difference between the predicted and experimental results may be due to a number of issues. During the practical bending process, springback is not only closely related to the shape, performance, bending radius, bending angle, neutral layer variations and tube wall thickness. It also has a significant relationship with the bending method, die structure, friction state and other parameters. However, these effects are ignored in our analytic model. Furthermore, during the practical NC tube bending process, cross-sectional flattening will occur, and the smaller the relative bending radius or the larger the bending angle, the larger the flattening that occurs. Flattening will lead to decreased springback. However, this flattening effect was also neglected in our analytic model. The relative bending radius of

the $D12 \text{ mm} \times t0.9 \text{ mm} \times \rho24 \text{ mm}$ bent tube is 2 and that of the $D6 \text{ mm} \times t0.6 \text{ mm} \times \rho18 \text{ mm}$ bent tube is 3. This means that more cross-sectional flattening will occur for the bent tube with the relative bending radius of 2. This will cause a larger error for that tube, which is why the error for the $D12 \text{ mm} \times t0.9 \text{ mm} \times \rho24 \text{ mm}$ bent tube is larger than for the $D6 \text{ mm} \times t0.6 \text{ mm} \times \rho 18\text{mm}$ bent tube. In addition, though thicknesses from our analytic model and the experiments vary similarly, there is difference between them with the maximum error of about 4% at $\varphi=90^\circ$ (Fig. 5). This difference in thickness variation would also bring about disparities in springback angle between the predicted and experimental results.

4.4 Springback model application

As Eq. (46) showing, the springback angle has a relationship with the initial tube geometric sizes (including the outside diameter, D , and wall thickness, t_0), material properties (including the strength coefficient, K , hardening exponent, n , and Poisson ratio, ν) and bent tube geometric sizes (including the relative bending radius, ρ/D). The influence and significance of these parameters on the springback angle were obtained using the analytic springback model developed in this study, as shown in Fig. 12. In the analyses, taking the initial geometric size, material properties and geometric size of the $D6 \text{ mm} \times t0.6 \text{ mm} \times \rho 18\text{mm}$ Ti-3Al-2.5V bent tube as reference values, parameters float 5% and 10% upward and downward based on their respective reference values, except for the relative bending radius, which varies within the range of the normal bending radius, from 2-4.

Figs. 12a, c and f show that the springback angle increases nearly uniformly with increases in the tube's outside diameter, strength coefficient and relative bending radius. These increasing trends become more obvious as the bending angle further increases. These results indicate a coupling effect between the tube's outside diameter, strength coefficient, relative bending radius and bending angle on the springback angle.

Figs. 12b, d and e illustrate that the springback angle decreases almost uniformly with increases in wall thickness, hardening exponent, Poisson ratio and the decreasing trend increases with the increase in bending angle. These results indicate a coupling effect between the wall thickness, hardening exponent, Poisson ratio and bending angle on the springback angle. Figs. 12d and e show that various hardening exponents and Poisson ratios have minimal effects on the springback angle.

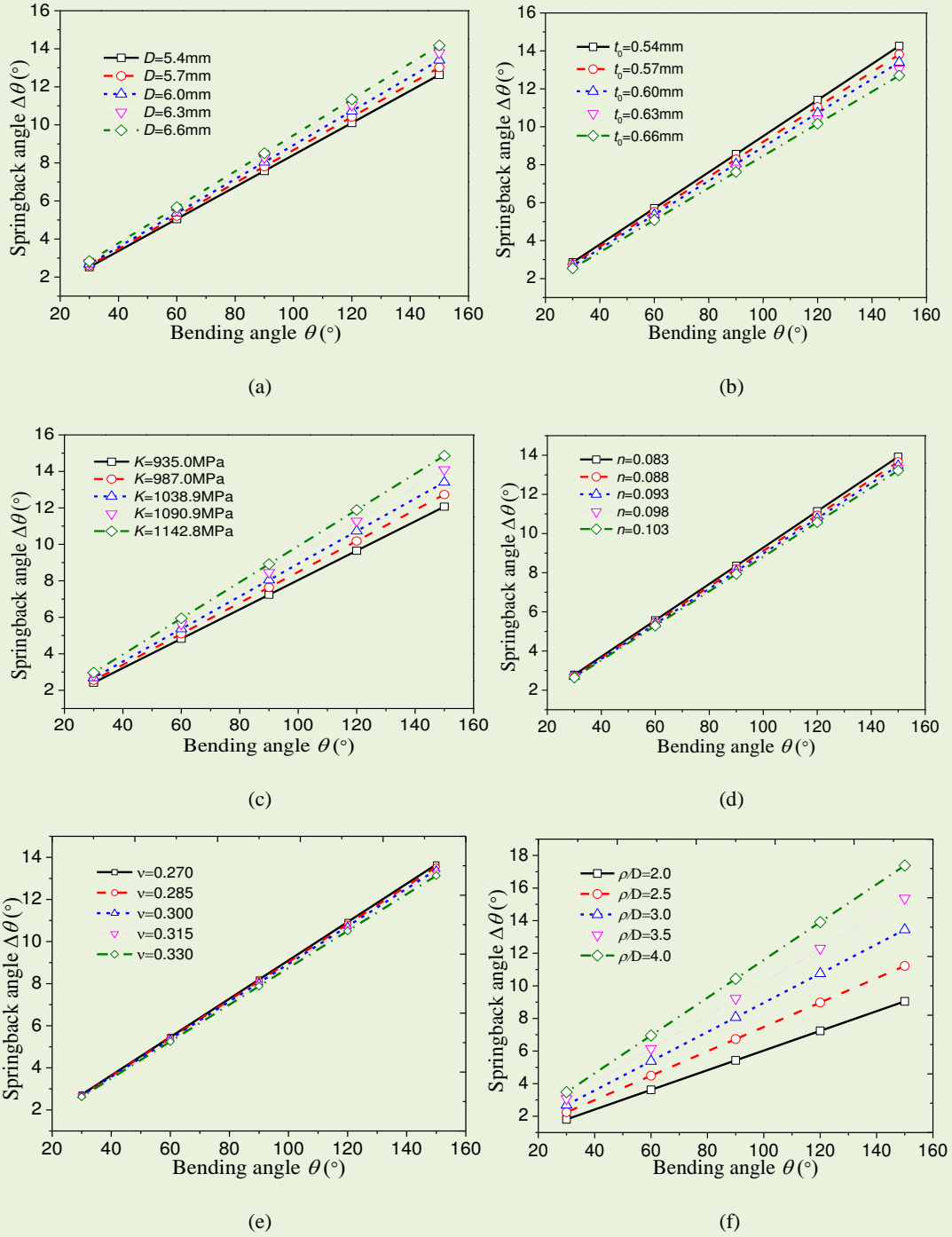


Fig. 12 Springback angle variations with the tube's outside diameters (a), wall thicknesses (b), strength coefficient (c), hardening exponent (d), Poisson ratio (e) and relative bending radius (f).

5. Conclusions

An analytic elastic-plastic tube bending springback model was established based on the static equilibrium condition. In the model, Young's modulus E , wall thickness t and neutral layer D_e variations were considered. Using the model, springback angle variation laws for Ti-3Al-2.5V tubes were obtained under various conditions. The main results are as follows:

(1) The springback angles, which considered these variations individually or combinedly, increase and approach the experimental results compared to the results that did not account for these variations. For a D_6 mm \times t0.6 mm Ti-3Al-2.5V tube, the prediction error was decreased by 1.0%, 24.5% and 43.9% when only considering E, D_e and t, respectively; by 26.3%, 46.3% and 67.4% when considering both D_e and E, t and E and D_e and t, respectively; and by 67.5% when considering all three variations.

(2) The t variation has the largest impact on the springback angle, decreasing the error by more than 40%. This was due to that the non-uniform thickness from the outermost to the innermost tube, resulting in an axial stress that decreased before springback, increased during and after springback, and a decrease and an increase in the area of outside and inside deformation zones, respectively. The contribution from D_e ranks as the second most influential, decreasing errors by more than 20%. This is because D_e variations cause opposing stress and area of deformation zone variations trends as those caused by t variations.

(3) The E variation contribution is the least significant, as the minimal variations between the initial value, E_0 , and stable value, E_a , only caused a slight decrease in the unloading slope of the plastic deformation zone. Furthermore, the influence of E_a on the springback is more obvious than that of E_0 because the affecting range of E_a is larger than that of E_0 . Therefore, the E variations can be neglected for the springback of tubes with a small difference between E_0 and E_a and bent under a normal bending radius. While for tubes with large differences between E_0 and E_a , and high springback prediction requirements, the E variations should be replaced by E_a .

(4) The springback angle of Ti-3Al-2.5V tubes obtained using the model increased nearly linearly with the increase in tube's outside diameter, strength coefficient and relative bending radius, as well as with the decrease in wall thickness, hardening exponent and Poisson ratio. However, the hardening exponent and Poisson ratio had little impact on the springback angle.

Acknowledgements

The authors acknowledge support from the National Science Fund for Excellent Young Scholars of China (Project 51222509), National Natural Science Foundation of China (Project 51175429) and Research Fund of the State Key Laboratory of Solidification Processing (Projects 97-QZ-2014 and 90-QP-2013). The authors also acknowledge the partial support of the Marie Curie International Research Staff Exchange Scheme (IRSES, MatProFuture, project no: 318968) within the 7th EC Framework Programme (FP7).

References

- Al-Qureshi, H. A., 1999. Elastic-plastic analysis of tube bending. *Int. J. Mach. Tool. Manu.* 39(1), 87-104.
- Al-Qureshi, H. A., Russo, A., 2002. Spring-back and residual stresses in bending of thin-walled aluminum tubes. *Mater. Des.* 23(2), 217-222.
- Chatti, S., Hermi, N., 2011. The effect of non-linear recovery on spring-back prediction. *Comput. Struct.* 89(13), 1367-1377.
- E, D. X., Guo, X. D., Ning, R. X., 2009a. Analysis of strain neutral layer displacement in tube-bending process. *J. Mech. Engineer.* 45(03), 307-310. (in Chinese)
- E, D. X., He, H. H., Liu, X. Y., Ning, R. X., 2009b. Spring-back deformation in tube bending. *Int. J. Miner. Metall. Mater.* 16(2), 177-183.
- Gu, R. J., Yang, H., Zhan, M., Li, H., Li, H. W., 2008. Research on the spring-back of thin-walled tube NC bending based on the numerical simulation of the whole process. *Comput. Mater. Sci.* 42(4), 537-549.
- Hencky, H., 1924. Zur Theorie plastischer deformationen und der hierdurch im material hervorgerufenen nachspannungen. *ZAMM - Z. Angew. Math. Me.* 4 (4), 323-334.
- Huang, T., Zhan, M., Yang, H., Guo, J., Tan, J. Q., 2015. A constitutive model for anisotropic tubes incorporating the variation of contractile strain ratio with deformation. *Int. J. Mech. Sci.* 90, 33-43.
- Hudovernik, M., Staupendahl, D., Gharbi, M., 2013. 3D numerical analysis of 2D profile bending with the torque superposed spatial bending method. *Stroj. Vestn.- J. Mech. Eng.*, 59(3), 139-147.
- Jiang, Z. Q., Yang, H., Zhan, M., Xu, X. D., Li, G. J., 2010a. Coupling effect of material properties and the bending angle on the spring-back angle of a titanium alloy tube during numerically controlled bending. *Mater. Des.* 31(4), 2001-2010.
- Jiang, Z. Q., Yang, H., Zhan, M., Yue, Y. B., Liu, J., Xu, X. D., Li, G. J., 2010b. Establishment of a 3D FE model for the bending of a titanium alloy tube. *Int. J. Mech. Sci.* 52, 1115-1124.
- Jiang, Z. Q., Zhan, M., Yang, H., Xu, X. D., Li, G. J., 2011. Deformation behavior of medium-strength TA18 high-pressure tubes during NC bending with different bending radii. *Chinese. J. Astron.* 24(5), 657-664.
- Li, H., Yang, H., Song, F. F., Zhan, M., Li, G. J., 2012. Spring-back characterization and behaviors of

- high-strength Ti-3Al-2.5V Tube in cold rotary draw bending. *J. Mater. Process. Technol.* 212(9), 1973-1987.
- Liao, J., Xue, X., Lee, M. G., Barlat, F., Gracio, J., 2014. On twist springback prediction of asymmetric tube in rotary draw bending with different constitutive models. *Int. J. Mech. Sci.* 89, 311-322.
- Megharbel, A. E., Nasser, G. A. E., Domiaty, A. E., 2008. Bending of tube and section made of strain-hardening materials. *J. Mater. Process. Technol.* 203(203), 372-380.
- Murata, M., Kuboki, T., Takahashi, K., Goodarzi, M., Jin, Y., 2008. Effect of hardening exponent on tube bending. *J. Mater. Process. Technol.* 201(1), 189-192.
- Paulsen, F., Welo, T., 1996. Application of numerical simulation in the bending of aluminium-alloy profiles. *J. Mater. Process. Technol.* 58(2), 274-285.
- Stachowicz, F., 2000. Bending with upsetting of copper tube elbows. *J. Mater. Process. Technol.* 100(1-3), 236-240.
- Tang, N.C., 2000. Plastic-deformation analysis in tube bending. *Int. J. Pres. Ves. Pip.* 77(12), 751-759.
- Xue, X., Liao, J., Vincze, G., Gracio, J. J., 2015. Modelling of mandrel rotary draw bending for accurate twist springback prediction of an asymmetric thin-walled tube. *J. Mater. Process. Technol.* 216, 405-417.
- Zhan, M., Huang, T., Yang, H., 2015. Variation of contractile strain ratio of Ti-3Al-2.5V tubes and its effects in tubes numerical control bending process. *J. Mater. Process. Technol.* 217, 165-183.
- Zhan, M., Huang, T., Zhang, P. P., Yang, H., 2014. Variation of Young's modulus of high-strength TA18 tubes and its effects on forming quality of tubes by numerical control bending. *Mater. Des.* 53, 809-815.